

# Orientation dependence in multiple ionization of He<sub>2</sub> and Ne<sub>2</sub> induced by fast, highly charged ions: Probing the impact-parameter-dependent ionization probability in 11.37-MeV/u S<sup>14+</sup> collisions with He and Ne

H.-K. Kim,<sup>1,\*</sup> H. Gassert,<sup>1</sup> J. N. Titze,<sup>1</sup> M. Waitz,<sup>1</sup> J. Voigtsberger,<sup>1</sup> F. Trinter,<sup>1</sup> J. Becht,<sup>1</sup> A. Kalinin,<sup>1</sup> N. Neumann,<sup>1</sup> C. Zhou,<sup>2</sup> L. Ph. H. Schmidt,<sup>1</sup> O. Jagutzki,<sup>1</sup> A. Czasch,<sup>1</sup> M. Schöffler,<sup>1</sup> H. Merabet,<sup>3</sup> H. Schmidt-Böcking,<sup>1</sup> T. Jahnke,<sup>1</sup> H. J. Lüdde,<sup>4</sup> A. Cassimi,<sup>2</sup> and R. Dörner<sup>1</sup>

<sup>1</sup>*Institut für Kernphysik, University Frankfurt, Max-von-Laue-Str. 1, 60438 Frankfurt, Germany*

<sup>2</sup>*CIMAP Caen, GANIL, Bd Henri Becquerel, BP 55027 14076 Caen Cedex 05, France*

<sup>3</sup>*Department of Mathematics, Statistics and Physics, College of Arts and Sciences, P.O. Box: 2713 Doha, Qatar*

<sup>4</sup>*Institut für Theoretische Physik, University Frankfurt, Max-von-Laue-Str. 1, 60438 Frankfurt, Germany*

(Received 3 December 2013; published 7 February 2014)

We investigate orientation effects in the fragmentation of He<sub>2</sub> and Ne<sub>2</sub> induced by S<sup>14+</sup> projectiles at an impact energy of 11.37 MeV/u. Multiple ionization shows a strong dependence on the orientation of the dimer axis with respect to the projectile beam axis. We attribute these effects to the impact-parameter-dependent ionization probability  $P(b)$  for the atomic scattering process S<sup>14+</sup> + He and S<sup>14+</sup> + Ne and compare our data with a Monte Carlo simulation.

DOI: [10.1103/PhysRevA.89.022704](https://doi.org/10.1103/PhysRevA.89.022704)

PACS number(s): 34.50.Fa

## I. INTRODUCTION

Ion-atom collisions are frequently treated in a semiclassical approach in which the projectile ion is described as a classical particle moving on a trajectory characterized by an impact parameter to the nucleus of the target. The response of the electronic wave function to the perturbation caused by the projectile is then calculated quantum mechanically. The impact parameter itself, however, is not an observable. All that can be measured in an experiment is the momentum transfer to the projectile, i.e., its deflection. For small impact parameters this deflection is mainly due to the interaction with the charged nucleus. Hence for high impact energies the impact parameter can be related to the Rutherford scattering angle  $\vartheta_{\text{Rutherford}}(b)$  of the projectile in a Coulomb potential. However, in outer valence shell ionization of atoms, which is the governing process, the momentum of the ejected electron corrupts the unambiguous assignment of the impact parameter to the scattering angle [1,2]. Thus except for very close collisions (e.g., in inner shell or core ionization as in [3]) the impact parameter is not directly measurable through momentum transfers.

In ion-molecule collisions, apart from the momentum transfer, another observable was proposed to be influenced by the impact parameter, which is the molecular orientation dependence. Pioneering theoretical and experimental works [4–7] studied orientation effects<sup>1</sup> in multiple electron ionization of covalent bound molecules. In particular, Werner *et al.* [8] measured the orientation-dependent multiple ionization yield of N<sub>2</sub> by He<sup>+</sup> impact.

It was shown that the probability of high degrees of ionization exhibits a strong dependence of the alignment of the molecules with respect to the projectile beam, while for low degrees of ionization no such effect occurs. The theoretical analysis was done in a simple model in which the molecule is

described as the sum of two independent atoms and the ionization process is treated in the independent electron approximation. Good agreement was shown in a quantitative comparison to the experiment which was made in a modified version of the statistical energy deposition model [9,10]. Within this framework these orientation effects were ascribed to geometric reasons caused by the nonisotropic electron density distribution within a molecule [5]. High degrees of ionization require a large energy deposition. In order to deposit a large amount of energy the electron density distribution probed by the projectile has to be high. This, in turn, is given for projectile trajectories close to the molecular axis (small impact parameters), which is the case when the molecule is oriented parallel to the projectile beam axis. Similarly, in studies by Caraby *et al.* [7] multiple ionization of CO was predicted to exhibit a strong molecular orientation, which is caused by small impact parameters.

Very recently Titze *et al.* [11] suggested accessing the impact parameter in ion-atom collisions by studying collisions between an ion and van der Waals dimers. Similarly to the case of covalently bound molecules the cross section for the reaction (transfer ionization, electron transfer) was observed to be dependent on the orientation of the dimer axis with respect to the incoming projectile beam  $N(\theta_{\text{mol}})$ . In contrast to collisions with covalent bound molecules in collisions with van der Waals bound rare-gas dimers, the “atomic” impact parameter dependence of a process can be directly associated with the orientation dependence. For rare-gas dimers, and in particular for He<sub>2</sub>, studied by Titze *et al.*, the approximation of two well-separated atoms is expected to be almost ideally satisfied. This is due to the low binding energy (only about 95 neV for He<sub>2</sub>) and the large mean internuclear distances (52 Å [12] for He<sub>2</sub>). Simultaneously the angular information of the fragmentation process is preserved.

In the straight-line approximation the impact parameter  $b$  is defined as the shortest distance from the nucleus of the target atom to the projectile trajectory. Thus  $P(b)$  is the probability that a projectile will interact with an atom at distance  $b$ . Figure 1 shows the calculated impact-parameter-dependent

\*kim@atom.uni-frankfurt.de

<sup>1</sup>Here we do not address the orientation effects due to interference phenomena.

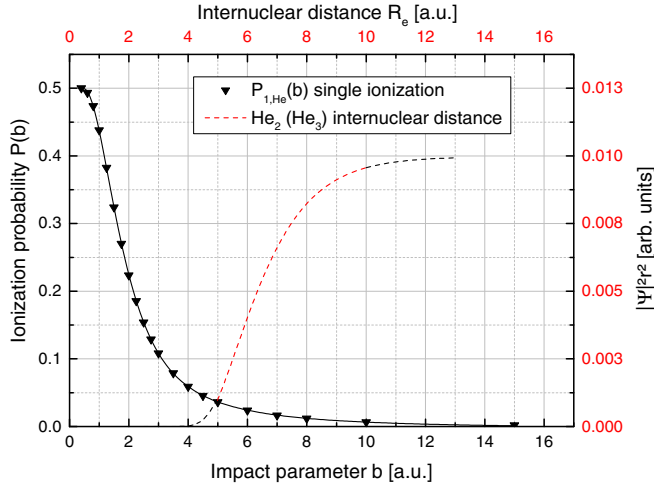


FIG. 1. (Color online) Calculated impact-parameter-dependent ionization probability for single ionization  $P_{1,\text{He}}(b)$  (filled triangles) in the collision system  $\text{S}^{14+} + \text{He}$  at a projectile energy of 11.37 MeV/u. The solid black line is a function fitted to the  $P(b)$ , which was obtained in an effective single-particle approximation [15]. Black, bottom axis: impact parameter. Black, left axis: impact-parameter-dependent ionization probability  $P(b)$ . The long-dashed line indicates the distribution of the internuclear distance in the ground-state helium dimer. The lighter (red) section of the long-dashed line was used in the simulation. Red, top axis: internuclear distance  $R$ . Red, right axis: internuclear distance distribution  $|\Psi_{\text{He}_2}|^2 r^2$  [13].

single-ionization probability [ $P_{1,\text{He}}(b)$ ; filled black triangles] in (11.37 MeV/u)  $\text{S}^{14+} + \text{He}$  collisions. Figure 2 correspondingly shows the single-, double-, and triple-ionization probabilities [ $P_{1,\text{Ne}}(b)$ , open black squares;  $P_{2,\text{Ne}}(b)$ , filled black triangles; and  $P_{3,\text{Ne}}(b)$ , open black circles, respectively] in (11.37 MeV/u)  $\text{S}^{14+} + \text{Ne}$  collisions.

The calculations are based on a time-dependent density functional model of a many-electron system in the  $x$ -only approximation [15,16]. It can be seen that each channel has its maximum ionization probability at different impact parameters. The decrease in  $P(b)$  at small impact parameter values is due to the dominance of higher ionization states for such close collisions.

Also, the maximum distance  $b_{\text{max}}$  up to which ionization is possible varies. Using these  $P(b)$  values one can directly obtain the expected angular distribution of those dimers which get ionized by interaction of the projectile with each of the two atoms. Obviously, close collision of the projectile with both atoms can only occur if the dimer is aligned almost parallel to the projectile axis. Therefore reaction channels with narrow  $P(b)$  will correspond to a strongly aligned breakup.

From these  $P(b)$  for each combination of final ionization states the dependence on the angle between the dimer axis and the projectile direction can be simulated as we show in Sec. IV. For simplicity of the argument we first assume a step function for the  $P(b)$  with a cutoff at  $b_{\text{max}}$ .

The probabilities for the various reaction channels which are possible in an ion-atom collision (e.g., single- and double-electron capture or single and double ionization) usually show different dependencies of the impact parameter. Thus in an ion-dimer collision the probabilities of the two individual

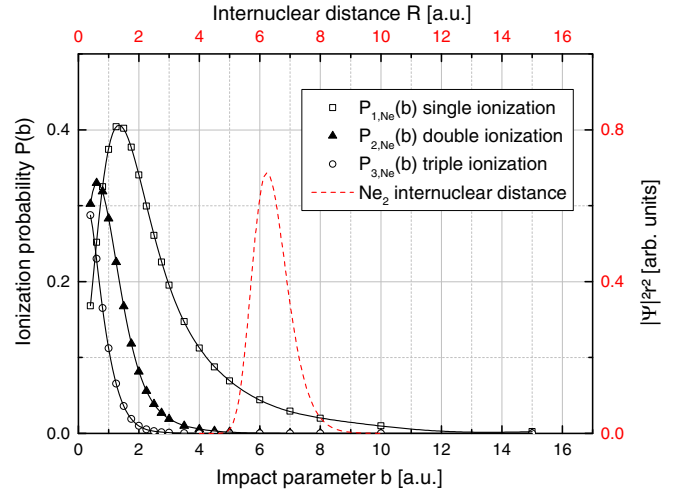
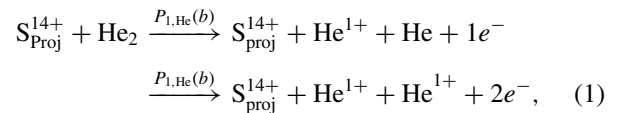


FIG. 2. (Color online) Calculated impact-parameter-dependent ionization probability for single ionization  $P_{1,\text{Ne}}(b)$  (open squares), double ionization  $P_{2,\text{Ne}}(b)$  (filled triangles), and triple ionization  $P_{3,\text{Ne}}(b)$  (open circles) in the collision system  $\text{S}^{14+} + \text{Ne}$  at a projectile energy of 11.37 MeV/u. The solid black lines are functions fitted to the  $P(b)$ , which were obtained in an effective single-particle approximation [15]. Black, bottom axis: impact parameter. Black, left axis: impact-parameter-dependent ionization probability  $P(b)$ . The long-dashed line (red) indicates the distribution of the internuclear distance in the ground-state neon dimer. Red, top axis: internuclear distance  $R$ . Red, right axis: internuclear distance distribution  $|\Psi_{\text{Ne}_2}|^2 r^2$  [14].

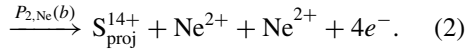
interactions of the projectile with each of the dimer's atoms will exhibit different  $b$  dependencies  $P_a(b) \neq P_b(b)$ , if the reaction process of the first interaction differs from that of the second one. This implies that only in the case of two subsequent ionization processes with the same degree of ionization does only one  $P(b)$  need to be considered, because  $P_a(b) = P_b(b) = P(b)$ .

In the experiment by Titze *et al.* the reaction channels “double capture” and “transfer ionization” in  $\text{He}^{2+} + \text{He}_2$  collisions were investigated at a projectile ion energy of 150 keV/u. For double capture and transfer ionization, however, the charge state of the projectile changes during the process, which also changes the  $P(b)$ . In the present work we build on the suggestion from Titze *et al.* but study multiple ionization of  $\text{He}_2$  and  $\text{Ne}_2$  by ion impact at a much higher projectile energy. The case of swift (11.4 MeV/u), highly charged ( $\text{S}^{14+}$ ) ions as projectiles is much simpler and more transparent. The major advantage of the chosen projectile energy is that the ionization channel is dominant. Accordingly, electron capture and projectile loss are negligible, which is crucial in order to test a single  $P(b)$ . This can be seen for the  $b$ -dependent single-ionization probability of a helium atom in the reaction pathway displayed in Eq. (1),



and for the double-ionization probability of the neon atom displayed in Eq. (2),





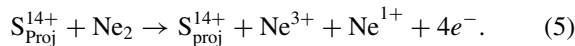
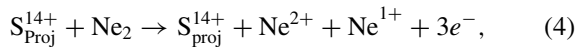
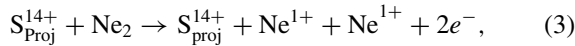
Neon dimers with a mean internuclear distance of 3.4 Å are still approximated well by two independent atoms. In these reactions the projectile almost instantaneously ionizes both centers of the dimer in two independent interactions. Accordingly the two remaining charged recoil ions Coulomb explode at an internuclear distance close to the equilibrium bond length of the dimer. This fragmentation mechanism, where the projectile interacts with both atoms of the dimer independently, is hereafter referred to as the Coulomb explosion (CE). It is in competition with other reaction channels where the projectile interacts with only one site of the dimer and the second atom is ionized later by an inner dimer process which we discuss below (Sec. III).

Due to the preservation of the projectile charge state after the first ionization process with the probability  $P_{1,\text{He}}(b)$  in Eq. (1) and  $P_{2,\text{Ne}}(b)$  in Eq. (2), the second interactions have the same impact parameter dependencies.

In the reaction channels  $\text{Ne}^{1+} + \text{Ne}^{1+}$ ,  $\text{Ne}^{2+} + \text{Ne}^{1+}$ , and  $\text{Ne}^{3+} + \text{Ne}^{1+}$  the angular distributions show a much more isotropic behavior than predicted by the computer simulation for CE. In a simple model we show that this effect can be reproduced by superimposing the contributions of other fragmentation mechanisms to the angular distribution. Due to the availability of all channels in one experiment, systematic errors are reduced in this approach.

## II. EXPERIMENT

The examined reaction channels of  $\text{S}^{14+}$  at a projectile energy of  $E_{\text{proj}} = 11.37$  MeV/u in collision with  $\text{He}_2$  are given by Eq. (1), and those in collision with  $\text{Ne}_2$  by Eq. (2), and



The measurement was performed with a COLTRIMS (cold target recoil ion momentum spectroscopy) momentum reaction microscope [17,18] at the medium energy beam line SME in cave  $D_1$  of the heavy-ion accelerator facility GANIL in Caen, France.  $\text{S}^{14+}$  projectiles with an energy of 11.37 MeV/u (projectile velocity  $v_{\text{proj}} = 21.2$  a.u.) were provided in bunches 1 ns in length, collimated to approximately 2 mm in diameter at intervals of 81.2 ns. The reaction takes place in the interaction region of a few cubic millimeters, which is formed in the beam overlap of the ionic projectile beam and the target gas jet. The precooled ( $\sim 14$  K for helium and  $\sim 150$  K for neon) target gas is further cooled in a supersonic gas expansion through a nozzle ( $\sim 5$  μm) at a driving pressure of about 1.5 b for helium and 11 b for neon. Two skimmers ( $\sim 0.3$  mm) reduce the gas jet diameter to 1–1.5 mm in the interaction region. A dimer-to-monomer fraction of approximately 1% is estimated. For helium the applied driving pressure and nozzle temperature lead to an additional contribution of  $\text{He}_3$  in the target jet [19]. However, the shapes of the distributions of the helium dimers' and trimers' internuclear distances are predicted to almost coincide for small distances [20]. The data analysis was thus performed for these corresponding regions. The created charged particles

are guided by weak, homogeneous electric and magnetic fields onto two time- and position-sensitive microchannel plate (75-mm-active-detection-diameter) detectors [21,22] located at the ends of the momentum spectrometer. The time-of-flight direction, which is parallel to the electric and magnetic field vector, the projectile beam axis, and the propagation direction of the target gas jet are pairwise orthogonal. The positions and flight times of at least two ions and one electron are detected in coincidence with a bunch marker signal from which the three-dimensional momenta are reconstructed. From the momenta the energies and the emission angles of the particles are calculated. The majority of statistical background events is suppressed in the data analysis by making use of the momentum conservation of the Coulomb exploding ions.

## III. FRAGMENTATION MECHANISMS

The goal of the present study is to investigate the ionization of both centers of the dimer by two independent sequential interactions of the projectile with the dimer, which is followed by CE. This is, however, not the only reaction pathway through which two ions can be created [11,23–26]. According to the nomenclature used in [23] the sequential ionization discussed so far is referred to as CE. The two additional channels are termed “interatomic Coulombic decay” (ICD) and “radiative charge transfer” (RCT).

The underlying principle in the reactions is similar for the lowest final states of ionization [Eqs. (1) and (3)] in the investigated dimer systems  $\text{He}_2$  and  $\text{Ne}_2$  as well as for the higher degrees of ionization which are populated in the neon dimer [Eqs. (2), (4), and (5)]. The reaction pathways are thus illustrated in more detail only for the example of the fragmentation channel given by Eq. (3). Figure 3 schematically shows the different possible fragmentation pathways of a ground-state neon dimer resulting in the Coulomb-exploding ion pair  $\text{Ne}^{1+} + \text{Ne}^{1+}$ .

In the first decay mechanism, CE, the projectile ion ionizes both atoms of the dimer in two subsequent steps. The Coulomb repulsion of the two charged target ions occurs instantly after the ionization. Due to the high velocity of the projectile the projectile-target interaction time is shorter than the vibrational period of the nuclei. Hence, in principle, the CE starts from the internuclear distance which the dimer has at the instant it is hit by the projectile.

For each fragmentation channel  $\text{Ne}^{n+} + \text{Ne}^{m+}$  with  $(n,m) := \{(1,1),(2,1),(3,1),(2,2)\}$  we therefore consider a kinetic energy release within the reflection approximation [27]  $E_{\text{KER}} = nm/R$ , with  $R$  being the internuclear distance. The initial distribution of  $R$  at which the ionization process takes place is given by the ground state of the dimer (for  $\text{Ne}_2$ :  $R_{\text{Ne}} \in [3 \text{ a.u.}, 10 \text{ a.u.}]$  and for  $\text{He}_2$ :  $R_{\text{He}} \in [5 \text{ a.u.}, 500 \text{ a.u.}]$ ). Not all internuclear distances, however, lead to the same probability of getting ionized for both atoms. This is accounted for in our simulation presented in Sec. IV.

The second fragmentation process is ICD, which occurs additionally in some channels. ICD, which was predicted by Cederbaum *et al.* in 1997 [28] and experimentally discovered in 2003 and 2004 [29,30], is an autoionization process by which an excited species can relax via transferring its excess energy to a neighboring atom where a low-energy electron

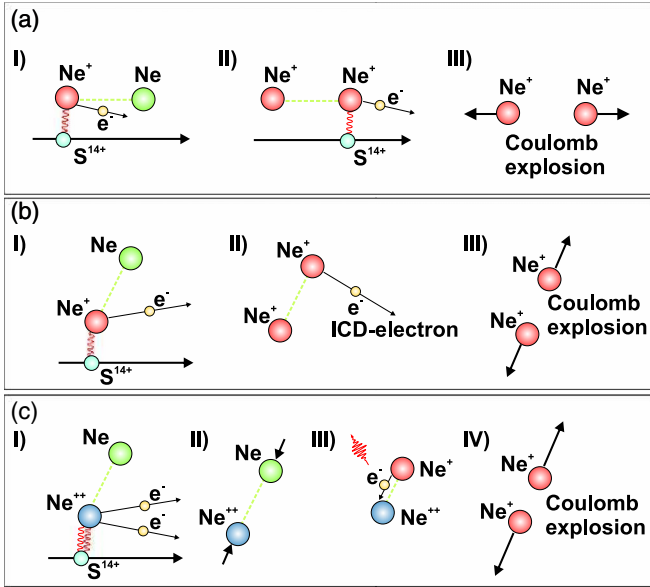


FIG. 3. (Color online) Ion-induced decay mechanisms in  $\text{Ne}_2$  resulting in the fragmentation channel  $\text{Ne}^{1+} + \text{Ne}^{1+}$ . (a) In the “direct” Coulomb explosion process the projectile subsequently ionizes both centers of the dimer, followed by Coulomb explosion. (b) In interatomic Coulombic decay (ICD) the projectile only ionizes one atom of the dimer, leaving it in an excited ionic state. The excited target ion relaxes by transferring its excess energy to the neighboring, neutral atom of the dimer. There a low-energy electron is emitted. (c) In the radiative charge transfer one of the neon atoms is doubly ionized in the initial interaction with the projectile. The  $\text{Ne}_2^{2+}$  dimer ion shrinks until one electron of the neutral atom transfers to the already doubly ionized site under the emission of a photon. The resulting singly charged neon atoms fragment in a Coulomb explosion.

is ejected. This process has been extensively studied both theoretically and experimentally (see [31,32] for recent review articles).

In the present model system ( $\text{Ne}_2$  fragmenting into  $\text{Ne}^{1+} + \text{Ne}^{1+}$ ) ICD progresses as follows: One of the neon dimer’s atoms is ionized by the removal of an innervalence  $2s$  electron (ionization potential  $\text{IP}_{2s} = 48.47$  eV) by ion impact, thus leading to a singly charged  $\text{Ne}^{+*}(2s^1 2p^6)$  state. The other atom remains in the neutral ground state  $\text{Ne}(2s^2 2p^6)$ . A  $2p$  electron of the excited cation fills the  $2s$  hole, releasing an excess energy of 26.91 eV. This energy is transferred to the neighboring neutral atom, where a  $2p$  outervalence electron, the ICD electron ( $e_{\text{ICD}}$ ), is ionized ( $\text{IP}_{2p} = 21.56$  eV). The remaining energy of 5.35 eV is shared among the kinetic energy release  $E_{\text{KER}}$  of the positively charged ion pair  $\text{Ne}^{1+} + \text{Ne}^{1+}$  and the kinetic energy of the ICD electron  $E_{e_{\text{ICD}}}$ . It thus follows that the sum energy is constant:<sup>2</sup>

$$E_{\text{sum,Ne}_2} = E_{\text{KER}} + E_{e_{\text{ICD}}} = \text{const} = 5.35 \text{ eV}. \quad (6)$$

In neon dimers ICD is known to be very fast (between 85 and 168 fs [33–35]). It occurs almost at the equilibrium inter-

nuclear distance of the dimer, without significant motion of the nuclei. This is the reason why ICD is indistinguishable from CE in  $E_{\text{KER}}$  [25]. ICD was also shown to occur in the larger  $\text{He}_2$  [11,36], whereby the ICD rate scales with the internuclear distance as  $1/R^6$  [37]. Thus for  $\text{He}_2$  ICD predominantly takes place, with preceding nuclear motion, at distances significantly shorter than the internuclear distance distribution of the helium dimer’s ground state [36]. Accordingly, most of the ICD in  $\text{He}_2$  takes place at times longer than 600 fs, up to several nanoseconds [38].

In the third process, RCT, one site of the dimer is initially doubly ionized by the projectile. The internuclear distance of the  $\text{Ne}_2^{2+}$  dimer ion decreases until one electron from the neutral atom transfers to the  $\text{Ne}^{2+}$  ion under the emission of a photon [39]. Here the CE is preceded by the contraction of the dimer, which leads to a higher  $E_{\text{KER}}$ . The same mechanism applies to RCT in the helium dimer [11].

#### IV. SIMULATION

The calculated  $P(b)$  are now used as input variables in a Monte Carlo simulation, which is also described in [11] and [40], in order to compare the calculated angular distributions to the experimental results. We calculate

$$F(\cos(\theta)) = \int_0^\infty \int_0^\infty \int_{-\infty}^\infty (P_a(b_1) \cdot P_b(b_2) \cdot P(R)) dx dy dR, \quad (7)$$

in a high number of simulated collision events (of the order of  $10^6$  trajectories per bin). Here  $\cos(\theta)$  is the angle of the dimer axis with respect to the projectile axis,  $P_a(b_1)$  and  $P_b(b_2)$  are the impact-parameter-dependent interaction probabilities of the projectile with each of the dimer’s atoms, and  $P(R)$  is the probability of finding the dimer at an internuclear distance  $R$  as depicted in Figs. 1 and 2. The impact parameters  $b_1$  and  $b_2$  of the projectile to the dimer nuclei (see Fig. 4) are

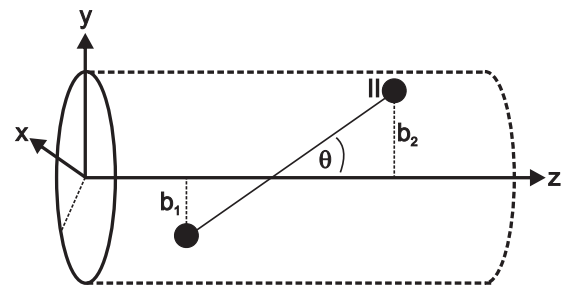


FIG. 4. The projectile trajectory is given by the  $z$  axis. The circle with radius  $r = b_{\text{max}}$  in the  $xy$  plane (perpendicular to the  $z$  axis) defines the area in which the atoms have to be located in order to be ionized.  $\theta$  is the orientation of the dimer with respect to the projectile beam axis.  $\cos(\theta) = 0$  therefore corresponds to a perpendicular orientation of the dimer to the projectile beam axis, and  $\cos(\theta) = \pm 1$  to a parallel orientation. The closest distances between the nuclei of the dimer to the projectile trajectory are called the impact parameters  $b_1$  and  $b_2$ . For dimers with an internuclear distance  $R > 2 \cdot b_{\text{max}}$  both atoms can only interact with the projectile when the molecule is oriented along the  $z$  axis.

<sup>2</sup>A more detailed description of ion-induced ICD occurring in the fragmentation channels which are denoted by Eqs. (3) and (4) is given in [26].

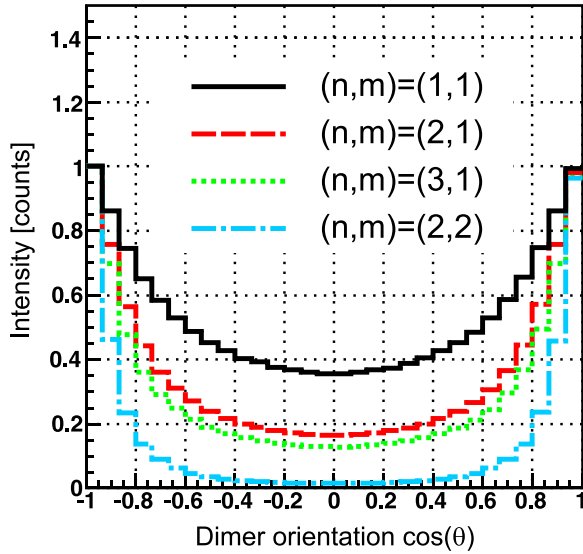


FIG. 5. (Color online) Calculated angular distributions of the dimer axis with respect to the ion beam axis [ $\cos(\theta) = \pm 1$  corresponds to the orientation parallel to the ion beam] for the Coulomb explosion process in the various ionization channels  $\text{Ne}^{1+} + \text{Ne}^{1+}$  (solid black curve),  $\text{Ne}^{2+} + \text{Ne}^{1+}$  [dashed (red) curve],  $\text{Ne}^{3+} + \text{Ne}^{1+}$  [dotted (green) curve], and  $\text{Ne}^{2+} + \text{Ne}^{2+}$  [dash-dotted (blue) curve]. Curves are normalized to the leftmost bin.

given by

$$b_{1,2} = \sqrt{\left(x \pm \frac{R}{2} \cos \theta\right)^2 + y^2}, \quad (8)$$

whereby  $x$  and  $y$  are the coordinates of the projectile in the plane perpendicular to the projectile beam. In histograms as, e.g., in Fig. 5, each bin corresponds to an interval in the angular tilt of the dimer axis. The function  $[F \cos(\theta)]$  is determined in  $N$  collisions as follows: In the first step for each collision event the internuclear distance of the dimer is randomly generated following the probability distribution  $P(R)$  of the ground-state dimer. For the same event the position of the projectile ( $x$  and  $y$ ) is generated homogeneously in the plane perpendicular to its direction of propagation, which then defines the collision geometry, the impact parameters  $b_1$  and  $b_2$  according to Eq. (8), and also  $P_a(b_1)$  and  $P_b(b_2)$ . The sum  $\sum_{i=1}^N P_a(b_1) \cdot P_b(b_2)$  over all collision events  $N$  determines the interaction probability. This procedure is repeated for each bin and the distribution is finally normalized to the sum of total counts obtained in the experiment.

### A. Coulomb explosion

In the simulation for the neon dimer the  $P(b)$  shown in Fig. 2 are combined according to the degree of ionization in the subsequent reaction processes. For  $\text{Ne}^{1+} + \text{Ne}^{1+}$  breakup induced by CE the sum  $\sum_{i=1}^N P_a(b_1) \cdot P_b(b_2)$  is chosen to be  $\sum_{i=1}^N P_{1,\text{Ne}}(b_1) \cdot P_{1,\text{Ne}}(b_2)$ . In the asymmetric  $\text{Ne}^{2+} + \text{Ne}^{1+}$  channel the  $P(b)$  in the simulation were chosen as  $\sum_{i=1}^N P_{2,\text{Ne}}(b_1) \cdot P_{1,\text{Ne}}(b_2)$ . This was done analogously for the  $\text{Ne}^{3+} + \text{Ne}^{1+}$ ,  $\text{Ne}^{2+} + \text{Ne}^{2+}$ , and also the CE-induced fragmentation of the helium dimer. As an example Fig. 5 shows the calculated angular distributions for the CE process in the

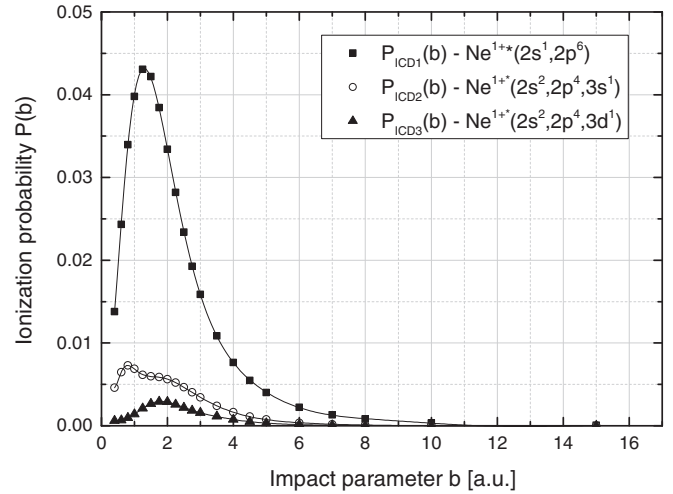


FIG. 6. ICD1, ICD2, and ICD3: calculated impact-parameter-dependent ionization probabilities for the neon atom in the collision system described in Fig. 2. The populated electronic configurations are denoted  $\text{Ne}^{1+}(2s^1 2p^6)$  [ $P_{\text{ICD1}}(b)$ ; filled black squares],  $\text{Ne}^{1+}(2s^2, 2p^4, 3s^1)$  [ $P_{\text{ICD2}}(b)$ ; open black circles], and  $\text{Ne}^{1+}(2s^2, 2p^4, 3d^1)$  [ $P_{\text{ICD3}}(b)$ ; filled black triangles]. Solid black lines are functions fitted to the  $P(b)$ .

various ionization channels:  $\text{Ne}^{1+} + \text{Ne}^{1+}$  (solid black curve),  $\text{Ne}^{2+} + \text{Ne}^{1+}$  [dashed (red) curve],  $\text{Ne}^{3+} + \text{Ne}^{1+}$  [dotted (green) curve], and  $\text{Ne}^{2+} + \text{Ne}^{2+}$  [dash-dotted (blue) curve]. The curves are normalized to the leftmost bin and show a stronger anisotropy for higher degrees of ionization.

## B. Interatomic Coulombic decay

ICD is simulated by considering the ion-induced population of the initial excited state which is required for the decay process. The corresponding inclusive probabilities are calculated from the one-particle density matrix according to [41–43].

### 1. $\text{Ne}^{1+} + \text{Ne}^{1+}$

ICD leading to the singly charged neon ions is triggered dominantly by the  $\text{Ne}^{1+}(2s^1 2p^6)$  state [ $P_{\text{ICD1}}(b)$  in Fig. 6]. We thus utilize  $P_a(b_1) = P_{\text{ICD1}}(b_1)$  for the first interaction. In the second interaction of the projectile with the dimer we use the impact-parameter-dependent probability  $P_e(b)$  (see Fig. 7), which is the probability that no ionization takes place. The sum is thus generated by  $\sum_{i=1}^N P_{\text{ICD1}}(b_1) \cdot P_e(b_2)$ . The second interaction is dealt with accordingly for all ICD channels. Thus in the following, only the creation of the excited state in the interaction of the projectile with the first atom is described.

In the same  $E_{\text{KER}}$  region ICD has been reported to occur also after the ionization of a  $2p$  electron with simultaneous excitation of a second  $2p$  electron. We therefore also consider the dipole-allowed shakeup states  $\text{Ne}^{1+}(2s^2, 2p^4, 3s^1)$  [ $P_{\text{ICD2}}(b)$  in Fig. 6] and  $\text{Ne}^{1+}(2s^2, 2p^4, 3d^1)$  [ $P_{\text{ICD3}}(b)$  in Fig. 6], which decay via virtual photon exchange [44].

### 2. $\text{Ne}^{2+} + \text{Ne}^{1+}$

In this asymmetric breakup channel numerous ICD channels were identified after irradiation with synchrotron light [39]. According to Kreidi *et al.* [39] about 75% of

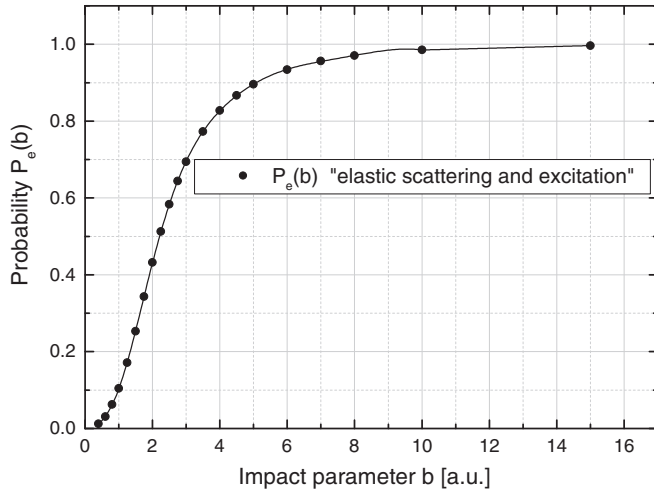


FIG. 7. Elastic scattering and excitation: calculated impact-parameter-dependent probability for the neon atom in the collision system described in Fig. 2. Filled black circles show the probability of elastic scattering and excitation (no ionization). The solid black line is a function fitted to the  $P(b)$ . Bottom axis: impact parameter. Left axis: impact-parameter-dependent ionization probability  $P(b)$ .

the  $\text{Ne}^{2+}(2s^1, 2p^5)[^1P]^3$  state [ $P_{\text{ICD4}}(b)$  in Fig. 8] and the  $\text{Ne}^{2+}(2s^0, 2p^6)$  [ $P_{\text{ICD5}}(b)$  in Fig. 8] contribute via ICD and ICD-like mechanisms to the angular distributions in the evaluated  $E_{\text{KER}}$  region.

### 3. $\text{Ne}^{3+} + \text{Ne}^{1+}$

In the  $\text{Ne}^{3+} + \text{Ne}^{1+}$  reaction channel also ICD was suggested to occur [26]. However, no theoretical calculations for this final channel are available up to now. In a simplistic approach we therefore model the decay process by assuming an initially excited  $\text{Ne}^{3+}(2s^1, 2p^4)$  [ $P_{\text{ICD6}}(b)$  in Fig. 9] state, which energetically allows for an ICD transition.

## V. RESULTS AND DISCUSSION

### A. Neon dimer

#### 1. Coulomb explosion

In order to obtain the angular distribution for the CE fragmentation channel, background events that stem from other decay mechanisms have to be suppressed. In the following this is illustrated in a little more detail for the fragmentation into  $\text{Ne}^{1+} + \text{Ne}^{1+}$ . Channels with a higher degree of ionization were treated accordingly.

Figure 10 shows the measured kinetic energy release for the fragmentation channel  $\text{Ne}^{1+} + \text{Ne}^{1+}$ . In the reflection approximation these kinetic energies  $E_{\text{KER}}$  correspond to the internuclear distances which are shown in Fig. 11, with the short-dashed (red) line indicating  $\text{Ne}_2$  in its ground state.

In Fig. 11 two pronounced peaks can be observed, whereby CE and ICD contribute to the right peak (about  $R = 6$  a.u.),

3. We base our calculations on the assumption that the triplet  $\text{Ne}^{2+}(2s^1, 2s^5)[^3P]$  is statistically populated three times as much as the singlet state  $\text{Ne}^{2+}(2s^1, 2p^5)[^1P]$ .

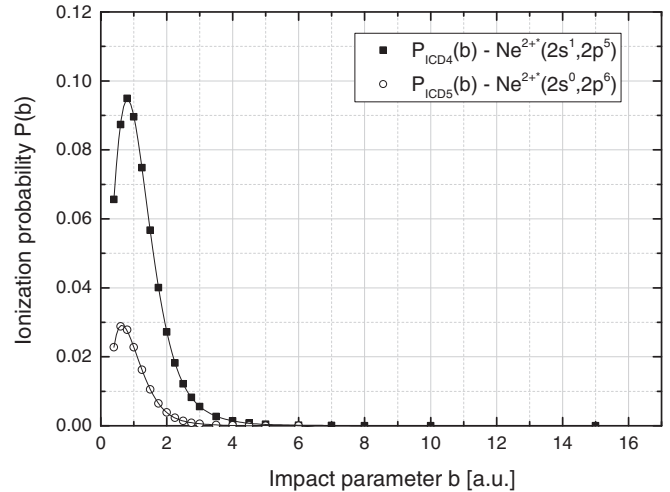


FIG. 8. ICD4 and ICD5: calculated impact-parameter-dependent ionization probabilities for the neon atom in the collision system described in Fig. 2. Populated electronic configurations are denoted  $\text{Ne}^{2+}(2s^1, 2p^5)[^1P]$  [ $P_{\text{ICD4}}(b)$ ; filled black squares], and  $\text{Ne}^{2+}(2s^0, 2p^6)$  [ $P_{\text{ICD5}}(b)$ ; open black circles]. Solid black lines are functions fitted to the  $P(b)$ .

while the left peak (about  $R = 3.7$  a.u.) is ascribed to events decaying via RCT. It can be seen that the CE and ICD are located in a region of the internuclear distance which is populated by the neon dimer, whereas RCT takes place at much smaller distances.

For our purposes the direct CE is the dissociation channel of interest because only in this process are two consecutive, independent interactions of the projectile with the atomic centers of the dimer necessary. Hence only the probability of this reaction channel will exhibit a dependency of the molecular alignment, which is related to a single, atomic  $P(b)$ .

Since CE is expected to occur only at internuclear distances of the  $\text{Ne}_2$  ground state, the analysis has to be restricted to

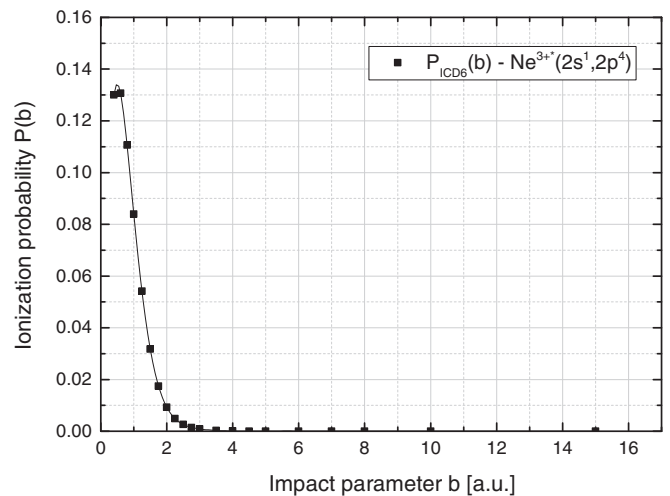


FIG. 9. ICD6: calculated impact-parameter-dependent ionization probabilities for the neon atom in the collision system described in Fig. 2. The populated electronic configuration is denoted  $\text{Ne}^{3+}(2s^1, 2p^4)$  [ $P_{\text{ICD6}}(b)$ ; filled black squares]. The solid black line is a function fitted to the  $P(b)$ .

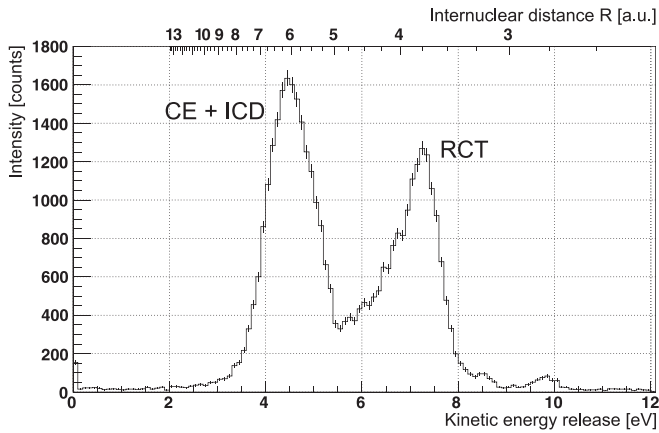


FIG. 10. Bottom axis: kinetic energy release distribution for a neon dimer fragmenting into  $\text{Ne}^{1+} + \text{Ne}^{1+}$ . Top axis: corresponding internuclear distance, calculated in the reflection approximation.

events within the respective  $E_{\text{KER}}$  region. Thus in the  $\text{Ne}^{1+} + \text{Ne}^{1+}$  breakup channel RCT can be omitted in the following discussion.

Events from ICD and CE are not unambiguously separable in the  $E_{\text{KER}}$  alone. However, in the fragmentation channels denoted by Eqs. (3) and (4) the ICD channels have been extensively characterized both in theory and in experiment [30–32]. From these studies it is well known that in Eq. (3) ICD events always produce an ICD electron of low energy,  $E_{e,\text{ICD}} < 3$  eV. Thus in two-ion–two-electron coincidences, only CE events are obtained if both electrons have higher energies than the ICD electron. In the symmetric  $\text{Ne}^{1+} + \text{Ne}^{1+}$  breakup channel the energy of both electrons was chosen to be above 7.5 eV in order to also suppress potential ICD events from shakeup states [44]. The same threshold in the electron energy was selected for the asymmetric  $\text{Ne}^{2+} + \text{Ne}^{1+}$  channel to filter out ICD. In  $\text{Ne}_2$  only for the breakup channel resulting in the ion pair  $\text{Ne}^{2+} + \text{Ne}^{2+}$  the CE is the only fragmentation mechanism in the relevant  $E_{\text{KER}}$  region. Figure 12 shows the angular distribution for the ion pairs  $\text{Ne}^{1+} + \text{Ne}^{1+}$ ,  $\text{Ne}^{2+} + \text{Ne}^{1+}$ , and  $\text{Ne}^{2+} + \text{Ne}^{2+}$  for the CE process in a polar representation.

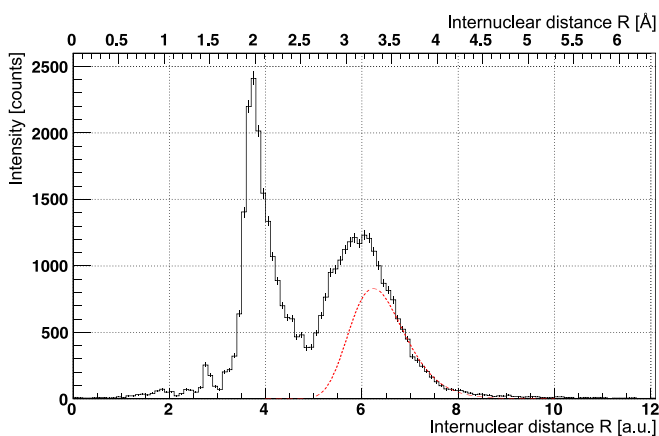


FIG. 11. (Color online) Internuclear distance, calculated in the reflection approximation for a neon dimer fragmenting into  $\text{Ne}^{1+} + \text{Ne}^{1+}$  (same data as in Fig. 10). The short-dashed (red) line indicates the ground-state distribution of the neon dimer  $|\Psi_{\text{Ne}_2}|^2 r^2$ .

Already the doubly ionized dimer [see Fig. 12(a)] exhibits a considerable anisotropy. With increasing degree of ionization ( $n + m = q = 3, 4$ ) the effect is strongly enhanced, which can be seen in Figs. 12(b) and 12(c), respectively.

Qualitatively the observed orientation-dependent ionization probability is interpreted by an intuitive geometrical picture given by Wohrer and Watson [5], which suggests a stronger ionization cross section along the projectile axis when the ratio of the radius (of the electron shell being ionized), compared to the internuclear separation, gets lower. In later theoretical and experimental studies by Kaliman *et al.* and Siegmann *et al.* [45,46] an orientation effect was expected if the condition

$$b_{\text{eff}} \leq R \quad (9)$$

is fulfilled, with  $b_{\text{eff}}$  being the impact parameters mostly contributing to the ionization.

Figure 2 shows that the  $P(b)$  in  $\text{S}^{14+} + \text{Ne}$  collisions readily meet the requirement formulated by Eq. (9). The  $P_{1,\text{Ne}}(b)$  has its maximum at small impact parameters (between 1 and 2 a.u.) with a steep decay behavior. Only the tail of the probability distribution extends to regions that are present in the ground-state internuclear distance distribution of the neon dimer. Hence this explains the orientation dependence of the dimer axis with respect to the projectile beam axis. The strength of this anisotropy can be influenced by changing the ratio  $b_{\text{eff}}/R$ . For the same collision system (same  $R$ ) this is achieved by changing the degree of ionization. Figure 2 shows that the relative probability of double ionization is higher for close collisions ( $b_{2,\text{Ne},P_{\text{max}}} \approx 0.6$  a.u.) than for single ionization ( $b_{1,\text{Ne},P_{\text{max}}} \approx 1.25$  a.u.), which extends to much higher impact parameters. Thus the probability of two double-ionization events is higher for dimers oriented strongly along the projectile trajectory. Accordingly, for two subsequent single-ionization processes the orientation effect is less pronounced. The intermediate orientation effect for the  $\text{Ne}^{2+} + \text{Ne}^{1+}$  breakup channel is caused by combining the contributing single- and double-ionization probabilities  $P_{1,\text{Ne}}(b)$  and  $P_{2,\text{Ne}}(b)$ . Thus the tendency of a stronger anisotropy with a higher degree of ionization can be observed.

## 2. Coulomb explosion + interatomic Coulombic decay

Figure 12, even though it displays events from CE only, is not well suited for a quantitative comparison with theory. This is because our gate on high electron energies introduces an uncontrolled bias on the impact parameter. High electron energies correspond preferentially to closer collisions than the low electron energies which are excluded by our gate in order to discriminate against ICD. For an unbiased comparison with theory we therefore will compare angular distributions generated without any gate on the electron energy with simulations which sum the contributions from ICD and CE. The data points in Fig. 13 depict these angular distributions integrated over all measured electron energies and therefore including ICD in Figs. 13(a)–13(c). In this one-dimensional histogram an isotropic distribution corresponds to a horizontal line.

In Figs. 13(a), 13(b), and 13(d) the experimental curve shapes show a behavior similar to that seen for the pure CE process in Fig. 12. The tendency of an enhanced anisotropy

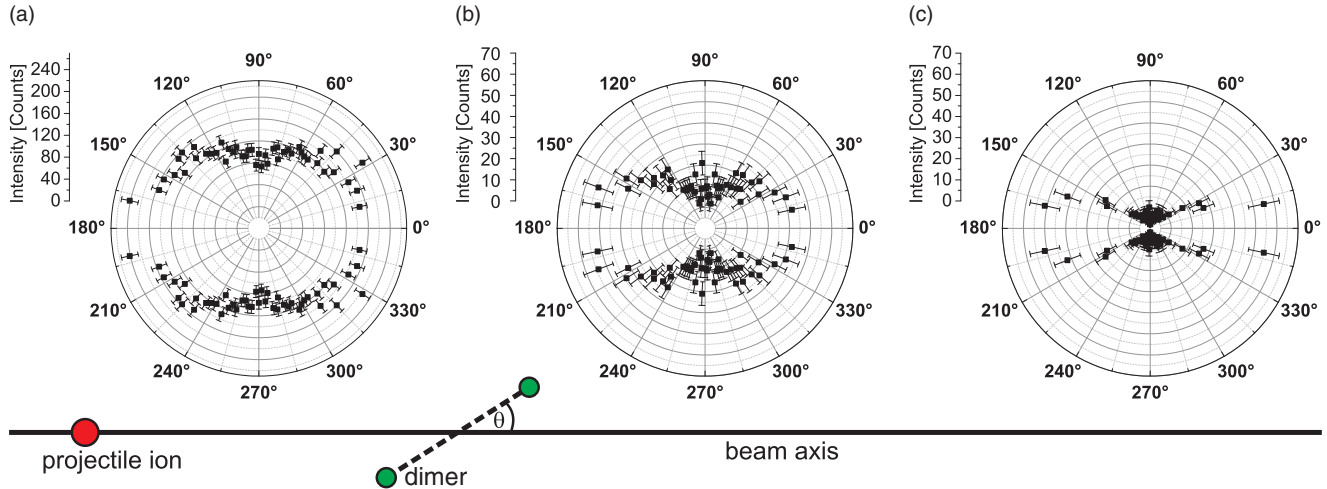


FIG. 12. (Color online) Angular distributions of the dimer axis from the direct Coulomb explosion are shown for  $S^{14+} + Ne_2$  collisions at a projectile impact energy of 11.37 MeV/u. An isotropic distribution (no angular dependence) corresponds to a circle with its center in the origin. Only the  $E_{KER}$  region was taken into account, which corresponds to the range of internuclear distances populated by the ground-state neon dimer. (a)  $Ne^{1+} + Ne^{1+}$  breakup channel with electron energies  $E_e > 7.5$  eV. (b)  $Ne^{2+} + Ne^{1+}$  breakup channel with electron energies  $E_e > 7.5$  eV. (c)  $Ne^{2+} + Ne^{2+}$  breakup channel.

towards higher degrees of ionization is observable. We compare these experimental distributions to a Monte Carlo simulation as described in Sec. IV. The dashed (blue) lines show the calculated angular distributions for the CE process. It can be seen that the anisotropy in the experimental data is less pronounced than the predicted curves for the CE process. We attribute this discrepancy to the contribution of ICD.

ICD is initiated by creating a one-sided excitation of the dimer, which typically takes place at low impact parameter values. Simultaneously, only elastic scattering and excitation (no ionization) may occur at the other constituent, for which the probability converges towards 1 at high impact parameter values. In the present scenario the simultaneous reaction at low impact parameter values at one center and high impact parameters at the second center leads to a favored population of dimer orientations perpendicular to the projectile beam axis.

In this representation of the histogram the angular distribution of ICD thus exhibits an inverse curvature to that of CE. By adding the angular distributions for ICD [dotted (red) curves and dash-dotted (green) curves] to the dashed (blue) curves for CE, the shape of the solid black curve (CE + ICD) reasonably reproduces the distribution of the experimental data. In Fig. 13(d) the simulated distribution is generated by the input of only  $P_{2,Ne}(b)$ . The curve is in good agreement with the data points, hence verifying the  $b$ -dependent ionization probability underlying our Monte Carlo simulation. The experiment in Fig. 13(d), however, shows a more isotropic behavior than the simulation, which particularly overestimates angles around  $\cos(\theta) = \pm 1$ . A possible explanation for this discrepancy is the reduced detection solid angle for electron energies  $E_e > 60$  eV in the experimental setup. The electron energy distribution for  $Ne^{1+}$  shows a steeper decay behavior towards higher

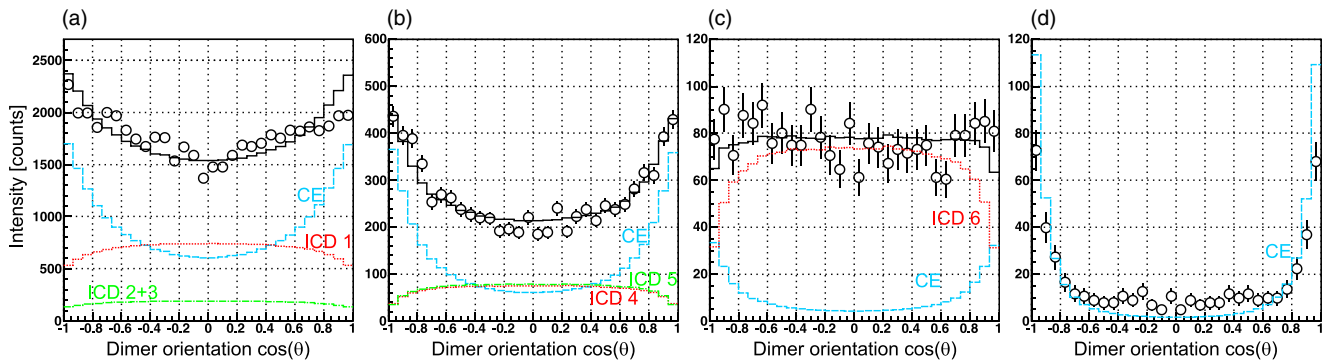


FIG. 13. (Color online) Angular distributions of the dimer axis integrated over all electron energies for  $S^{14+} + Ne_2$  collisions at a projectile impact energy of 11.37 MeV/u. An isotropic distribution (no angular dependence) corresponds to a straight horizontal line in this histogram. Only the  $E_{KER}$  region was taken into account, which corresponds to the range of internuclear distances populated by the ground-state neon dimer. (a)  $Ne^{1+} + Ne^{1+}$  breakup channel. (b)  $Ne^{2+} + Ne^{1+}$  breakup channel. (c)  $Ne^{3+} + Ne^{1+}$  breakup channel. (d)  $Ne^{2+} + Ne^{2+}$  breakup channel. For the CE process the dashed (blue) lines are generated in a Monte Carlo simulation (see text) using the  $P(b)$  as shown in Fig. 2. In addition to CE, the contributions of ICD are also modeled in the simulation [dotted (red) curves and dash-dotted (green) curves]. (a)–(c) Solid black curves are the sums of the other curves. The integral over each solid black curve is normalized to the number of counts in the experiment.

TABLE I. First row: simulated cross sections of the ionization channels divided by the cross section of the  $\text{Ne}^{1+} + \text{Ne}^{1+}$  breakup. Second row: corresponding experimental values corrected by the charge-state-dependent detection efficiency for the recoil ions and the number of electrons which are created in the reaction process. Third row: quotient from the first and second rows.

	$\frac{N(\text{Ne}^{1+} + \text{Ne}^{1+})}{N(\text{Ne}^{1+} + \text{Ne}^{1+})}$	$\frac{N(\text{Ne}^{2+} + \text{Ne}^{1+})}{N(\text{Ne}^{1+} + \text{Ne}^{1+})}$	$\frac{N(\text{Ne}^{3+} + \text{Ne}^{1+})}{N(\text{Ne}^{1+} + \text{Ne}^{1+})}$	$\frac{N(\text{Ne}^{2+} + \text{Ne}^{2+})}{N(\text{Ne}^{1+} + \text{Ne}^{1+})}$
Simulation	1	0.197	0.200	0.015
Experiment	1	0.150	0.043	0.009
Ratio ( $\frac{\text{simulation}}{\text{experiment}}$ )	1	1.313	4.651	1.667

electron energies than the doubly ionized ions  $\text{Ne}^{2+}$  [26]. Thus relatively more high-energy electrons are missing for the  $\text{Ne}^{2+} + \text{Ne}^{2+}$  channel. High-energy electrons are more likely to be produced in close collisions. Fragmentation events induced via CE at low impact parameter values in turn have a higher probability of occurring for dimers which are oriented along the projectile beam axis. The missing high-energy electrons caused by the decreased collection angle would therefore preferably contribute to events at  $\cos(\theta) = \pm 1$ .

The cross sections of the ionization channels which are calculated in the simulation are given in the first row in Table I in relation to the cross section of the  $\text{Ne}^{1+} + \text{Ne}^{1+}$  breakup. In the second row the corresponding experimental values are listed. The experimental values are corrected for the charge-state-dependent detection efficiency for the recoil ions and the number of electrons which are created in the reaction process. The third row lists the quotient from the theoretical and the experimental values and therefore indicates the discrepancy between the two. We attribute the large discrepancy for the  $\text{Ne}^{3+} + \text{Ne}^{1+}$  channel to a branching ratio (similar to the  $\text{Ne}^{2+} + \text{Ne}^{1+}$  channel) that has to be taken into account and is not known.

### B. Helium dimer

In the case of helium we assess regions of the internuclear distances  $R_{\text{He}} \in [5 \text{ a.u.}, 10 \text{ a.u.}]$ , which correspond to a kinetic energy of  $E_{\text{KER}} \in [2.7 \text{ eV}, 5.4 \text{ eV}]$ . In this range the shape of the internuclear distance distribution of the dimer closely resembles that of the pairwise distance distribution of two helium nuclei bound in a  $\text{He}_3$  [20]. Mainly events from CE populate the considered interval since ICD and RCT occur almost entirely at internuclear distances  $R < 5 \text{ a.u.}$  [11,36,38]. In addition, those events with a sum energy of  $E_{\text{sum,He}_2} = E_{\text{KER}} + E_{e,\text{ICD}} = 16.2 \pm 2.5 \text{ eV}$  (which is characteristic for ICD in the helium dimer) are suppressed for at least one measured electron. Therefore the remaining contribution of events decaying via ICD is estimated to be less than 13%.

Figure 14 shows the angular distribution for the helium dimers when a strong anisotropy is already observed in the  $\text{He}^{1+} + \text{He}^{1+}$  breakup. The size of the He atom is smaller than Ne and more tightly bound. This radial electron density probability as well as the binding energy in turn influences the  $P(b)$  distribution, which is also shifted towards smaller impact parameter values. At the same time the helium dimer's internuclear separation is more extended than that of the neon

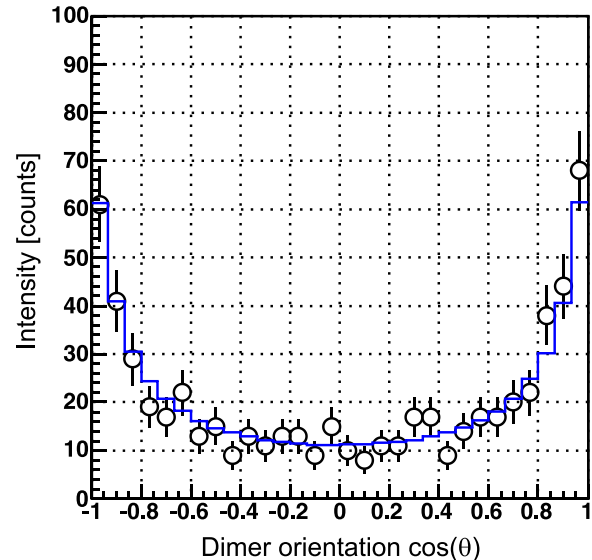


FIG. 14. (Color online) Angular distributions of the dimer axis from the direct Coulomb explosion are shown for  $\text{He}^{1+} + \text{He}^{1+}$  breakup in  $\text{S}^{14+} + \text{He}_2$  collisions at a projectile impact energy of 11.37 MeV/u. An isotropic distribution (no angular dependence) corresponds to a straight horizontal line in this histogram. For the  $\text{He}^{1+} + \text{He}^{1+}$  breakup channel, only the  $E_{\text{KER}}$  region was taken into account, which corresponds to the range of internuclear distances  $R_{\text{He}} \in [5 \text{ a.u.}, 10 \text{ a.u.}]$ . In addition, those events with a sum energy of  $E_{\text{sum,He}_2} = E_{\text{KER}} + E_{e,\text{ICD}} = 16.2 \pm 2.5 \text{ eV}$  (which is characteristic for ICD in the helium dimer) are suppressed for at least one measured electron. The solid (blue) line is generated in a Monte Carlo simulation (see text) using the  $P(b)$  as shown in Fig. 1 and normalized to the integral of the experimental histogram.

dimer. These effects lead to a lower average  $b_{\text{eff-to-R}}$  ratio for  $\text{S}^{14+} + \text{He}$  collisions than for  $\text{S}^{14+} + \text{Ne}$  for the same degree of ionization ( $q = 2$ ). The orientation effect can be expected to be more pronounced in the  $\text{He}^{1+} + \text{He}^{1+}$  channel than in the  $\text{Ne}^{1+} + \text{Ne}^{1+}$  breakup. The theoretical calculation, and with that the tested  $P_{1,\text{He}}(b)$ , show excellent agreement with the experimental data.

## VI. CONCLUSIONS

In conclusion we have measured the angular distribution of singly and multiply charged ion pairs from the collision  $\text{S}^{14+} + \text{Ne}_2$  and  $\text{S}^{14+} + \text{He}_2$ . These data have been used to test calculated impact parameter dependencies for the ionization of the atom. A good agreement between the simulation and the experiment was obtained for the helium dimers. For the neon dimers an overall good agreement was obtained but a stronger isotropic contribution in the experiment around  $\cos(\theta) = \pm 1$  was exhibited. In the fragmentation channels  $\text{Ne}^{1+} + \text{Ne}^{1+}$ ,  $\text{Ne}^{2+} + \text{Ne}^{1+}$ , and  $\text{Ne}^{3+} + \text{Ne}^{1+}$  the contributions of ICD lead to a more reduced anisotropy than predicted by our simulations for the pure, sequential two-center ionization process. In a simple model we have also calculated the angular distribution for the one-sidedly triggered ICD process, which shows a preference for dimers perpendicular to the projectile axis, i.e., the opposite trend to what one finds for two-center ionization. Taking the contribution of ICD into account in our simulation the

added angular distributions (CE + ICD) reproduce the shape of the experimental data. The calculated relative cross sections (between the ionization channels) and the relative cross sections obtained in the experiment are within the same order of magnitude. The largest discrepancy (Ne<sup>3+</sup> + Ne<sup>1+</sup> channel) is suggested to originate from the branching ratio for the decay routes of the excited Ne<sup>3+\*</sup>(2s<sup>1</sup>,2p<sup>4</sup>) state, which is not known.

## ACKNOWLEDGMENTS

We gratefully acknowledge the GANIL and CIMAP staff for their exceptional help during the experiment in Caen. This work was supported by the Koselleck Project of the DFG and by European Community FP7 Capacities—Integrated Infrastructure Initiative; ENSAR Contract No. 262010.

- 
- [1] R. Dörner, J. Ullrich, H. Schmidt-Böcking, and R. E. Olson, *Phys. Rev. Lett.* **63**, 147 (1989).
- [2] J. Ullrich, R. Olson, R. Dörner, V. Dangendorf, S. Kelbch, H. Berg, and H. Schmidt-Böcking, *J. Phys. B* **22**, 627 (1989).
- [3] H. Sharabati, K. Bethge, J. Ullrich, R. Dörner, R. E. Olson, V. Dangendorf, R. Koch, and H. Schmidt-Böcking, *J. Phys. B* **23**, 2957 (1990).
- [4] S. L. Varghese, C. L. Cocke, S. Cheng, E. Y. Kamber, and V. Frohne, *Nucl. Instrum. Methods Phys. Res. Sec. B* **40/41**, 266 (1989).
- [5] K. Wöhler and R. L. Watson, *Phys. Rev. A* **48**, 4784 (1993).
- [6] V. Horvat, O. Heber, R. L. Watson, R. Parameswaran, and J. M. Blackadar, *Nucl. Instrum. Methods Phys. Res. Sec. B* **99**, 94 (1995).
- [7] C. Caraby, A. Cassimi, L. Adoui, and J. P. Grandin, *Phys. Rev. A* **55**, 2450 (1997).
- [8] U. Werner, N. M. Kabachnik, V. N. Kondratyev, and H. O. Lutz, *Phys. Rev. Lett* **79**, 1662 (1997).
- [9] A. Russek and J. Meli, *Physica* **46**, 222 (1970).
- [10] C. L. Cocke, *Phys. Rev. A* **20**, 749 (1979).
- [11] J. Titze *et al.*, *Phys. Rev. Lett.* **106**, 033201 (2011).
- [12] R. E. Grisenti, W. Schöllkopf, J. P. Toennies, G. C. Hegerfeldt, T. Köhler, and M. Stoll, *Phys. Rev. Lett* **85**, 2284 (2000).
- [13] F. Luo, G. Kim, G. C. McBane, C. F. Giese, and W. R. Gentry, *J. Chem. Phys.* **98**, 9687 (1993).
- [14] Simona Scheit, private communications.
- [15] H. J. Lüdde, *Springer Ser. Atom. Opt. Plasma Phys.* **35**, 205 (2003).
- [16] T. Kirchner, H. J. Lüdde, and M. Horbatsch, *Recent Res. Dev. Phys.* **5**, 433 (2004).
- [17] R. Dörner, V. Mergel, O. Jagutzki, L. Spielberger, J. Ullrich, R. Moshhammer, and H. Schmidt-Böcking, *Phys. Rep.* **330**, 95 (2000).
- [18] J. Ullrich, R. Moshhammer, A. Dorn, R. Dörner, L. Ph. H. Schmidt, and H. Schmidt-Böcking, *Rep. Prog. Phys.* **66**, 1463 (2003).
- [19] L. W. Bruch, W. Schöllkopf, and J. P. Toennies, *J. Chem. Phys.* **117**, 1544 (2002).
- [20] E. Hiyama and M. Kamimura, *Phys. Rev. A* **85**, 022502 (2012).
- [21] O. Jagutzki, J. S. Lapington, L. B. C. Worth, U. Spillman, V. Mergel, and H. Schmidt-Böcking, *Nucl. Instrum. Methods Phys. Res. A* **477**, 256 (2002).
- [22] O. Jagutzki, V. Mergel, K. Ullmann-Pfleger, L. Spielberger, U. Spillmann, R. Dörner, and H. Schmidt-Böcking, *Nucl. Instrum. Methods Phys. Res. A* **477**, 244 (2002).
- [23] J. Matsumoto, A. Leredde, X. Flechard, K. Hayakawa, H. Shiromaru, J. Rangama, C. L. Zhou, S. Guillous, D. Hennecart, T. Muranaka, A. Mery, B. Gervais, and A. Cassimi, *Phys. Rev. Lett.* **105**, 263202 (2010).
- [24] J. Matsumoto, A. Leredde, X. Flechard, K. Hayakawa, H. Shiromaru, J. Rangama, C. L. Zhou, S. Guillous, D. Hennecart, T. Muranaka, A. Mery, B. Gervais, and A. Cassimi, *Phys. Scripta T* **144**, 014016 (2011).
- [25] H.-K. Kim *et al.*, *Proc. Natl. Acad. Sci. USA* **108**, 11821 (2011).
- [26] H. K. Kim, H. Gassert, M. S. Schöffler, J. N. Titze, M. Waitz, J. Voigtsberger, F. Trinter, J. Becht, A. Kalinin, N. Neumann, C. Zhou, L. P. H. Schmidt, O. Jagutzki, A. Czasch, H. Merabet, H. Schmidt-Böcking, T. Jahnke, A. Cassimi, and R. Dörner, *Phys. Rev. A* **88**, 042707 (2013).
- [27] E. A. Gislason, *J. Chem. Phys.* **58**, 3702 (1973).
- [28] L. S. Cederbaum, J. Zobeley, and F. Tarantelli, *Phys. Rev. Lett* **79**, 4778 (1997).
- [29] S. Marburger, O. Kugeler, U. Hergenhahn, and T. Möller, *Phys. Rev. Lett* **90**, 203401 (2003).
- [30] T. Jahnke, A. Czasch, M. S. Schöffler, S. Schössler, A. Knapp, M. Kász, J. Titze, C. Wimmer, K. Kreidi, R. E. Grisenti, A. Staudte, O. Jagutzki, U. Hergenhahn, H. Schmidt-Böcking, and R. Dörner, *Phys. Rev. Lett* **93**, 163401 (2004).
- [31] V. Averbukh, Ph. V. Demekhin, P. Kolorenc, S. Scheit, S. D. Stoychev, A. I. Kuleff, Y.-C. Chiang, K. Gokhberg, S. Kopelke, N. Sisourat, and L. S. Cederbaum, *J. Electron Spectrosc. Relat. Phenom.* **183**, 36 (2011).
- [32] U. Hergenhahn, *J. Electron Spectrosc. Relat. Phenom.* **184**, 78 (2011).
- [33] R. Santra and L. S. Cederbaum, *J. Chem. Phys.* **115**, 6853 (2001).
- [34] N. Vaval and L. S. Cederbaum, *J. Chem. Phys.* **126**, 164110 (2007).
- [35] K. Schnorr *et al.*, *Phys. Rev. Lett.* **111**, 093402 (2013).
- [36] T. Havermeier, T. Jahnke, K. Kreidi, R. Wallauer, S. Voss, M. Schöffler, S. Schössler, L. Foucar, N. Neumann, J. Titze, H. Sann, M. Kühnel, J. Voigtsberger, J. H. Morilla, W. Schöllkopf, H. Schmidt-Böcking, R. E. Grisenti, and R. Dörner, *Phys. Rev. Lett.* **104**, 133401 (2010).
- [37] R. Santra and L. S. Cederbaum, *Phys. Rep.* **368**, 1 (2002).
- [38] F. Trinter *et al.*, *Phys. Rev. Lett.* **111**, 093401 (2013).
- [39] K. Kreidi *et al.*, *Phys. Rev. A* **78**, 043422 (2008).
- [40] Jasmin Titze, Ph.D. thesis, Goethe Universität Frankfurt am Main, 2012.
- [41] H. J. Lüdde and R. M. Dreizler, *J. Phys. B* **18**, 107 (1985).
- [42] P. Kürpick, H. J. Lüdde, W. D. Sepp, and B. Fricke, *Z. Phys. D* **25**, 17 (1992).
- [43] T. Kirchner, H. J. Lüdde, and R. M. Dreizler, *Phys. Scripta T* **80**, 416 (1999).

- [44] T. Jahnke, A. Czasch, M. Schöffler, S. Schössler, M. Käs, J. Titze, K. Kreidi, R. E. Grisenti, A. Staudte, O. Jagutzki, L. P. H. Schmidt, Th. Weber, H. Schmidt-Böcking, K. Ueda, and R. Dörner, *Phys. Rev. Lett.* **99**, 153401 (2007).
- [45] Z. Kaliman, N. Orlic, N. M. Kabachnik, and H. O. Lutz, *Phys. Rev. A* **65**, 012708 (2001).
- [46] B. Siegmann, U. Werner, R. Mann, Z. Kaliman, N. M. Kabachnik, and H. O. Lutz, *Phys. Rev. A* **65**, 010704 (2001).